The Role of (tBuPOCOP)Ir(I) and iridium(III) Pincer Complexes in the Catalytic Hydrogenolysis of Silyl Triflates into Hydrosilanes

Gabriel Durin, Jean-Claude Berthet, Emmanuel Nicolas, Pierre Thuéry, Thibault Cantat

The Role of ($^{t\mathrm{Bu}}$POCOP)Ir(I) and iridium(III) Pincer Complexes in the Catalytic Hydrogenolysis of Silyl Triflates into Hydrosilanes

Gabriel Durin, Jean-Claude Berthet, Emmanuel Nicolas, Pierre Thuéry, and Thibault Cantat*

Université Paris-Saclay, CEA, CNRS, NIMBE, 91191 Gif-sur-Yvette Cedex, France

*Email: thibault.cantat@cea.fr

KEYWORDS: Iridium, Pincer Complexes, Catalysis, Hydrogenolysis, Reduction, Silyl Triflates, Hydrosilanes

ABSTRACT: Hydrosilanes are convenient reductants for a large variety of organic substrates, but they are produced via energy-intensive processes. These limitations call for the development of general catalytic processes able to transform Si–O into Si–H bonds. We report here the catalytic hydrogenolysis of R_3SiOTf (R = Me, Et, Ph) species in the presence of a base (e.g. NEt_3), by the hydride complexes [($^{t\mathrm{Bu}}$POCOP)IrH(X)] (X = H, OTf; ($^{t\mathrm{Bu}}$POCOP = [(1,3-C_6H_3)(OP*t*Bu)$_2$]). Syntheses and crystal structures of new iridium(I) and iridium(III) complexes are presented as well as their role in the R_3SiOTf to R_3SiH transformation. The mechanisms of these reactions have been examined by DFT studies, revealing that the rate-determining step is the base-assisted splitting of H_2

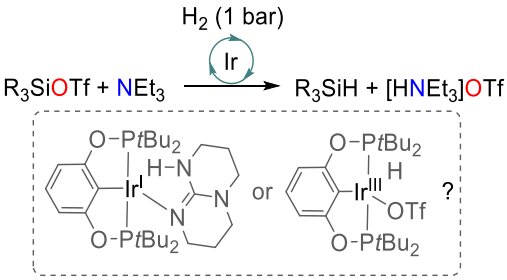

Introduction

The activation of siloxanes and silicon oxide derivatives is a key strategy to enter the value chain of silicon chemistry. While SiH_4 and $SiCl_4$ are the main starting blocks in the synthesis of silicon compounds, they require the use of silicon(0) obtained from energy intensive processes.[1] In contrast, the use and re-use of oxidized derivatives such as siloxanes, silanols and silicon (pseudo)halides is appealing to produce basic organosilicon synthons. Among them, hydrosilanes are mild and versatile reducing agents which are common industrial compounds for the synthesis or the functionalization of organosilicon polymers by dehydrocoupling reactions or hydrosilylation of alkenes.[2,3] In synthetic chemistry, they promote highly efficient and selective reactions such as the functionalization of inactivated C–H bonds in catalytic processes[4] or the reduction of carbonyl-containing molecules.[5–8] Recent studies have highlighted new utilizations for hydrosilanes to recover valuable molecules through C–O bond reduction/cleavage of oxygenated feedstock such as CO_2,[9] wood lignin[10] and plastics[11] toward a circular economy with low oil dependency. Currently, hydrosilane synthetic strategies rely on energy-intensive processes which involve strong reducing agents such as $LiAlH_4$.[12] Hydrogenolysis of Si–X bonds has been introduced by the groups of Hidai,[13,14] Shimada,[15,16] Schneider[17] and Cantat[18] as an alternative way to hydrosilanes and would be a convenient approach when using green H_2 generated *via* both electrochemical and photochemical splitting of water (Scheme 1).[19,20] Due to the paucity of work in this area, the development of novel systems favoring Si–X to Si–H conversion is crucial and their studies should give a better understanding of the intrinsic mechanism of such transformation.

In 1999 and 2003, Hidai *et al.* reported the catalytic hydrogenolysis of silyl enol ether into R_3SiH and ketones using [(dppe)$_2$RuCl(η^2-H_2)]OTf as catalyst under mild conditions (50 °C, 1 bar H_2). Although not focused towards the formation of hydrosilanes, this report demonstrated that hydrogenolysis can occur on Si–O linkages.[13,14]

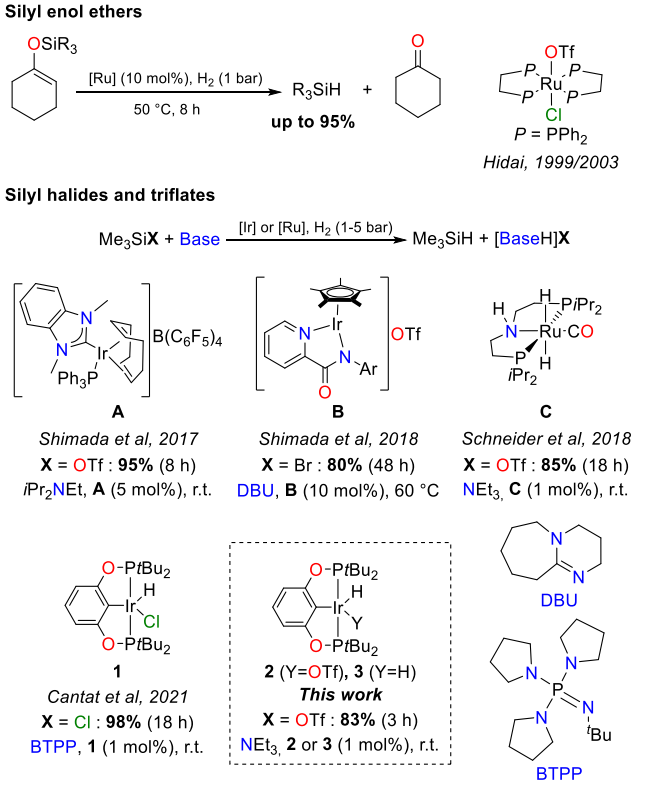

Scheme 1. Selected examples for the synthesis of hydrosilanes through catalytic hydrogenolysis of silyl enol ethers or halides.

In 2017 and 2018, the group of Shimada[15,16] described successful catalytic Si–X to Si–H transformations (X = OTf, I, Br) with iridium(III) complexes **A** and **B** (Scheme 1). The reactions require high catalytic charges (5−10 mol%) and the presence of an amine or amidine base such as N^{i}Pr$_2$Et or DBU (1,8-diazabicyclo[5.4.0]undec-7-ene). The reaction is sensitive to the steric hindrance of the R groups in $R_{4-n}SiX_n$ substrates and the reactivity of these silanes is following the leaving group ability of the X moiety in the order OTf > I > Br > Cl. The group of Schneider[17] also reported in 2018 excellent conversion and yields in Me_3SiH, Me_2SiH_2 or $Me_2SiH(OTf)$ from the corresponding triflates when catalyzed with ruthenium(II) pincer complex **C** (Scheme 1). Finally, our group recently reported the use of the iridium(III) pincer [($^{t\text{Bu}}$POCOP)IrHCl] (**1**) as an efficient catalyst in the hydrogenolysis of [Si]–Cl compounds when combined with superbases such as BTPP (BTPP = (*t*Bu-imino)tri(pyrrolidino)phosphorane).[18]

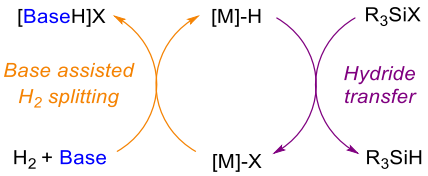

Scheme 2. Proposed mechanism for the catalytic hydrogenolysis of silyl halides and triflates.

The proposed mechanism for such a transformation can be split in two distinct parts (Scheme 2). First, the splitting of H_2 (left, in orange) at the metal center with a base that is strong enough to ensure the transformation of [M]–X into [M]–H bonds with the release of a salt. This reaction is particularly difficult when X = Br, Cl because of the inherent strengths of the [M]–X bonds. Second (right, in purple), the [M]–H complex transfers its hydride to the R_3Si–X species to yield the hydrosilane. The careful choice of the base and of the metal complex is crucial to induce a catalytic turnover. Because iridium pincer complexes such as **1** display good performances in both hydrogenation[21,22] and hydrosilylation reactions[23] by activating H–H and Si–H bonds, they should also be effective for the reverse reaction *i.e.* hydrogenolysis of silyl halides and triflates following the micro-reversibility principle in catalysis. Since various formal oxidation states of iridium (I to V) can be reached, a focus on the intermediates that may form during the reaction is of great interest. In this context, silyl triflates represent a good platform to study the hydrogenolysis mechanism.

We present here the catalytic hydrogenolysis of silyl triflates into the corresponding hydrosilanes using $^{t\text{Bu}}$POCOP pincer complexes of iridium(III) and iridium(I) with the presence of a nitrogen base. The chemical behavior of the potential iridium(III) precatalysts [($^{t\text{Bu}}$POCOP)IrH(X)] (X = H, Cl, OTf) was studied in presence of stoichiometric quantities or excess of the reagents H_2, R_3SiOTf and the base NEt_3 or TBDH (= 1,5,7-triazabicyclo[4.4.0]dec-5-ene) to explore the mechanism of the catalytic hydrogenolysis of silyl triflates. Synthesis and characterization of the complexes [($^{t\text{Bu}}$POCOP)Ir^{III}H(OTf)] (**2**), [($^{t\text{Bu}}$POCOP)Ir^{III}H(NCMe)$_2$]OTf (**5**), [($^{t\text{Bu}}$POCOP)IrH$_2$(TBDH)] (**6$_{cis}$**), [($^{t\text{Bu}}$POCOP)Ir^{I}(TBDH)] (**7**) and [($^{t\text{Bu}}$POCOP)Ir^{III}H(TBD)] (**8**) are presented, as well as several crystal structures. The experimental work has been coupled with DFT calculations to bring mechanistic insights for this reaction.

Experimental Section

General considerations. Me_3SiOTf, Et_3SiOTf and 1,5,7-triazabicyclo[4.4.0]dec-5-ene (TBDH), were purchased from Sigma-Aldrich, degassed and used as received. Commercial triethylamine was obtained from Carlo Erba. It was degassed, dried and then distilled prior to use. C_6D_6, Tol-d_8 and THF-d_8 were dried over sodium/benzophenone and vacuum-distilled before use. CD_3CN was dried over CaH_2, distilled before use, and stored over activated molecular sieves (4 Å). Molecular sieves (4 Å; Aldrich) was activated by prolonged drying (48 h) at 250 °C under primary dynamic vacuum. The iridium(III) complex [($^{t\text{Bu}}$POCOP)IrHCl] (**1**) was synthesized according to literature procedure[22] from commercial bis(1,5-cyclooctadiene)diiridium(I) dichloride ([(COD)IrCl]$_2$) and $^{t\text{Bu}}$POCOPH ([(1,3-C_6H_4)(OP*t*Bu)$_2$]), prepared from commercial resorcinol [(1,3-C_6H_4)(OH)$_2$] and ClP(*t*Bu)$_2$ (Sigma-Aldrich). Ph_3SiOTf was obtained from commercial Ph_3SiCl and AgOTf (Sigma-Aldrich) according to literature procedure.[23] All the syntheses were conducted under ultra-high purity argon with the rigorous exclusion of air and water (< 5 ppm oxygen or water), using standard Schlenk-vessel and vacuum-line techniques and an MBraun LabMaster DP inert atmosphere (Ar) glovebox. Glassware was dried overnight at 75°C or flame dried before use. Sterile syringe filter (0.2 µm Cellulose Acetate) were purchased from VWR. NMR spectra were recorded on a Bruker AVANCE Neo 400 MHz spectrometer at 25 °C unless otherwise stated. Chemical shifts (δ) values are referenced to solvent residual peaks (for ^{1}H and ^{13}C) or external reference (for ^{11}B, ^{19}F and ^{31}P) and reported in parts per million (ppm) relative to tetramethylsilane (^{1}H, ^{13}C), phosphoric acid (^{31}P), $BF_3{\cdot}OEt_2$ (^{11}B) or trifluoroacetic acid (^{19}F). Coupling constants (*J*) are given in Hz, multiplicities are named as singlet (s), doublet (d), triplet (t), quartet (q), multiplet or overlapping signals (m) and broad signal (br), solvent is given in parenthesis. GC-MS spectra were collected on a Shimadzu GCMS-QP2010 Ultra gas chromatograph mass spectrometer equipped with a Supelco SLB^{TM}-MS fused silica capillary (30 m x 0.25 mm x 0.25 µm). Elemental analyses of samples sealed under vacuum were performed under inert atmosphere by Medac Ltd at Chobham (Surrey, UK) or Analytische laboratorien at Lindlar (Germany).

Crystallography. The data were collected at 100(2) K on a Nonius Kappa-CCD area detector diffractometer[25] using graphite-monochromated Mo Kα radiation (λ = 0.71073 Å). The crystals were introduced into glass capillaries with a protective coating of Paratone-N oil (Hampton Research). The data (combinations of φ- and ω-scans with a minimum redundancy of at least 4 for 90% of the reflections) were processed with HKL2000.[25] Absorption effects were corrected empirically with SCALEPACK.[26] The structures were solved by intrinsic phasing with SHELXT,[27] expanded by subsequent difference Fourier synthesis and refined by full-matrix least-squares on F^2 with SHELXL.[28] All non-hydrogen atoms were refined with anisotropic displacement parameters. When present, the hydrogen atoms bound to iridium and nitrogen atoms were retrieved from residual electron density maps and were fully refined. The carbon-bound hydrogen atoms were introduced at calculated positions and were treated as riding atoms with an isotropic displacement parameter equal to 1.2 times that of the parent atom (1.5 for CH_3, with optimized geometry). The triflate anions in **2** and **4** are disordered, the two components having been refined with occupancy parameters constrained to sum to unity. Crystal data and structure refinement parameters are given in Table S2 (ESI, Section 2). The molecular plots were drawn with ORTEP-3.[29]

Computational details. Calculations were performed using the Gaussian16 suite of software.[30] The PBE0[31]-D3[32] functional was used in conjunction with the Def2TZVP[33–36] basis set for

Ir, the 6-311+G(d,p)[37–44] basis set for Si and mobile H atoms, and the 6–31G(d)[45–54] basis set for all other atoms. All geometries were fully optimized without any symmetry or geometry constrains. Harmonic vibrational analyses were performed to confirm and characterize the structures as minima or transition states. Free energies were calculated within the harmonic approximation for vibrational frequencies. The effects of the solvation by benzene were included in the energy calculations using the SMD model through single point calculations on the gas-phase optimized geometry.[55]

Catalytic Protocols

General procedure for the hydrogenolysis of silyl triflates: In a J. Young NMR tube, the iridium complex (1 mol%) was dissolved in 0.5 mL C_6D_6. The base (0.11 mmol) and the silyl triflate (0.10 mmol) were then successively added *via* syringe. The solution was degassed twice by freeze-pump-thaw cycles before being refrozen with liquid nitrogen and filled with H_2 (1 bar). The sample was thawed and immediately shaken. After 3–300 h at room temperature, the products were identified by ^{1}H NMR spectroscopy and quantified by relative integration of the R_xSi signals versus an internal standard (1,3,5-trimethylbenzene). Et_3SiH and Ph_3SiH were also quantified by GC-MS (see SI 1.4 for details).

Synthetic procedures

[(^{tBu}POCOP)IrH(OTf)] (**2**): In a glove box, **1** (200 mg, 0.32 mmol) and AgOTf (91 mg, 0.35 mmol) were dissolved in toluene (20 mL) in a 50 mL round bottom flask. The solution protected from light was stirred 14 h at room temperature (r.t.). and then filtered on a frit of porosity 4 and extracted with toluene (2x10 mL). The solvent was evaporated under vacuum affording **2** as an orange powder in 96 % yield (225 mg, 0.31 mmol). ^{1}H NMR (400 MHz, 23 °C, C_6D_6): 6.66 (t, 1H, J = 8.0 Hz, *p*-H_{Ar}), 6.56 (d, 2H, J = 8.0 Hz, *m*-H_{Ar}), 1.19 (vt, J_{P-H} = 10.8 Hz, 36H, ^{t}Bu), −42.88 (t, $^2J_{P-H}$ = 10.8 Hz, 1H, Ir−H). ^{13}C{^{1}H} NMR (100 MHz, C_6D_6): 162.81 (Cq, vt, J_{P-C} = 5.6 Hz, $C_{Ar-ortho}$), 123.74 (CH, $C_{Ar-para}$), 99.81 (CH, vt, J_{P-C} = 5.3 Hz, $C_{Ar-meta}$), 37.99 (Cq, vt, J_{P-C} = 12.5 Hz, 2 P(*t*Bu)$_2$), 34.15 (Cq, vt, J_{P-C} = 12.5 Hz, P(*t*Bu)$_2$), 22.18 (CH_3, vt, J_{P-C} = 3.1 Hz, P(*t*Bu)$_2$), 21.71 (CH_3, vt, J_{P-C} = 3.1 Hz, P(*t*Bu)$_2$). ^{19}F{^{1}H} (376 MHz, 23 °C, C_6D_6): −81.93. ^{31}P{^{1}H} NMR (162 MHz, 23 °C, C_6D_6): 177.0. Anal. Calcd for $C_{23}H_{40}F_3IrO_5P_2S$ (M = 739.79 g.mol^{-1}): C, 37.34; H, 5.45; F, 7.70. Found: C, 37.35; H, 5.43; F, 7.69.

[(^{tBu}POCOP)IrH(NCMe)$_2$]OTf (**5**)**:** In a 50 mL round bottom flask, **1** (200 mg, 0.32 mmol) was suspended in freshly distilled CH_3CN (10 mL). Me_3SiOTf (64 µL, 0.35 mmol, 1.1 eq) was then added *via* a syringe and the clear yellow solution obtained was stirred for 15 min at r.t. The solvent was removed under vacuum and the solid residue was washed with pentane (2 x 5 mL) to give **4** as a white yellowish powder isolated in 78 % yield (205 mg, 0.25 mmol). ^{1}H NMR (400 MHz, 23 °C, CD_3CN): 6.81 (t, 1H, J = 8.0 Hz, *p*-H_{Ar}), 6.46 (d, 2H, J = 8.0 Hz, *m*-H_{Ar}), 2.18 (s, 3H, CH_3CN*cis*), 1.99 (s, 3H, CH_3CN*trans*), 1.51 (vt, J_{P-H} = 6.4 Hz, 18H, *t*Bu), 1.31 (vt, J_{P-H} = 6.4 Hz, 18H, *t*Bu), −20.92 (t, $^2J_{P-H}$ = 8.2 Hz, 1H, Ir−H). ^{13}C{^{1}H} NMR (100 MHz, CD_3CN): 164.86 (Cq, vt, J_{P-C} = 5.5 Hz, $C_{Ar-ortho}$), 125.73 (CH, s, $C_{Ar-para}$), 104.97 (CH, vt, J_{P-C} = 5.2 Hz, $C_{Ar-meta}$), 41.37 (Cq, vt, J_{P-C} = 12 Hz, 2 P(*t*Bu)$_2$), 40.98 (Cq, vt, J_{P-C} = 12 Hz, P(*t*Bu)$_2$), 27.81 (CH_3, vt, J_{P-C} = 2.9 Hz, 2 P(*t*Bu)$_2$), 2 P(*t*Bu)$_2$), 27.16 (CH_3, vt, J_{P-C} = 2.9 Hz, 2 P(*t*Bu)$_2$). ^{19}F{^{1}H} (376 MHz, 23 °C, CD_3CN): −79.35. ^{31}P{^{1}H} NMR (162 MHz, 23 °C, C_6D_6): 162.27. Anal. Calcd for $C_{27}H_{46}F_3IrN_2O_5P_2S$ (M = 821.89 g.mol^{-1}): C, 39.46; H, 5.64; N, 3.41; F, 6.93. Found: C, 39.59; H, 5.66; N, 3.80; F, 7.36.

[(^{tBu}POCOP)IrH$_2$(TBDH)] (**6$_{cis}$**): A round bottom flask **(**20 mL) was charged with **1** (50 mg, 0.08 mmol) and TBDH (22 mg, 0.16 mmol, 2 eq), on which toluene (5 mL) was condensed. The initially red solution turned yellow with formation of a white deposit after a few minutes. The flask was filled with dihydrogen (1 bar) and the mixture stirred for 18 h at r.t. during which the solution turned orange. After addition of pentane (5 mL), to increase the precipitation of the salt [$TBDH_2$]Cl, the later deposit was discarded from the orange solution by filtration with a syringe filter (0.2 µm) and the product further extracted from the salt with a 1:1 mixture of pentane and toluene (2x5 mL). The orange solution was then evaporated to dryness and complex **6$_{cis}$** isolated as a pale orange powder (85 %, 49 mg, 0.067 mmol). ^{1}H NMR (400 MHz, C_6D_6): 8.68 (s, 1H, NH), 6.81 (m, 1H, *p*-H_{Ar}), 6.74 (m, 2H, *m*-H_{Ar}), 3.84 (m, 2H, TBDH(CH_2)), 2.74 (td, J = 5.9 Hz, 2.5 Hz, 2H, TBDH(CH_2)), 2.51 (t, J = 6.4 Hz, 2H, TBDH(CH_2)), 2.30 (t, J = 5.9 Hz, 2H, TBDH(CH_2)), 1.56 (vt, J = 6.6 Hz, 18H, P(*t*Bu)$_2$), 1.50 (vt, J = 6.6 Hz, 18H, P(*t*Bu)$_2$), 1.33 (m, 2H, TBDH(CH_2)), 1.17 (p, J = 5.9 Hz, 2H, TBDH(CH_2)), −9.16 (tdd, J_{P-H} = 14.7 and J_{H-H} = 11.4, 3.3 Hz, 1H, Ir−H), −9.59 (td, J_{P-H} = 17.7 and J_{H-H} = 11.4 Hz, 1H, Ir−H). ^{13}C{^{1}H} NMR (100 MHz, C_6D_6): 163.48 (Cq, t, J_{P-C} = 6.5 Hz, $C_{Ar-ortho}$), 149.59 (Cq, s, TBDH), 121.16 (CH, s, $C_{Ar-para}$), 118.29 (Cq, t, J_{P-C} = 5.2 Hz, $C_{Ar-ipso}$), 103.26 (CH, t, J_{P-C} = 5.5 Hz, $C_{Ar-meta}$), 59.88 (CH_2, s, TBDH), 48.79 (CH_2, s, TBDH), 48.20 (CH_2, s, TBDH), 40.55 (CH, t, J_{P-C} = 12.5 Hz, P(*t*Bu)$_2$), 39.03 (CH_2, s, TBDH), 38.16 (CH, t, J_{P-C} = 11.5 Hz, P(*t*Bu)$_2$), 28.58 (CH_3, t, J_{P-C} = 3.7 Hz, P(*t*Bu)$_2$), 28.44 (CH_3, t, J_{P-C} = 3.4 Hz, P(*t*Bu)$_2$), 24.45 (CH_2, s, TBDH), 22.70 (CH_2, s, TBDH). ^{31}P{^{1}H} NMR (162 MHz, C_6D_6): 167.99. Anal. Calcd for $C_{31}H_{55}IrN_4O_2P_2$ (M = 730.92 g.mol^{-1}): C, 47.65; H, 7.45; N, 5.75. Found: C, 47.84; H, 7.30; N, 5.62.

[(^{tBu}POCOP)Ir(TBDH)] (**7**) and [(^{tBu}POCOP)IrH(TBD)] (**8**): The orange complex **1** (50 mg, 0.08 mmol) and white TBDH (22 mg, 0.16 mmol, 2eq) were dissolved in toluene (5 mL) in a 20 mL round bottom flask. The resulting yellow solution containing a white deposit was stirred for 2 h at r.t. Pentane was then added to increase the salt deposit and the solution was filtered through a syringe filter (0.2µm). The product is further extracted from the salt with a 1:1 mixture of pentane and toluene (2x5 mL) and filtered as above. The yellow solution was evaporated to dryness to yield complexes **7** and **8** as yellow powder in 82 % yield (48 mg, 0.066 mmol). Anal. Calcd for $C_{29}H_{52}IrN_3O_2P_2$ (M = 728.92 g.mol^{-1}): C, 47.79; H, 7.19; N, 5.76. Found: C, 47.83; H, 7.33; N, 5.85. **7**: ^{1}H NMR (400 MHz, C_6D_6): 7.82 (s, 1H, NH), 7.03 (t, J =7.7 Hz, 1H, *p*-H_{Ar}), 6.91 (d, J = 7.7 Hz, 2H, *m*-H_{Ar}), 3.43 (m, 2H, TBDH(CH_2)), 2.75 (td, J = 5.9 Hz, 2.3 Hz, 2H, TBDH(CH_2)), 2.44 (t, J = 5.9 Hz, 2H, TBDH(CH_2)), 2.34 (t, J = 5.9 Hz, 2H, TBDH(CH_2)), 1.49 (vt, J = 6.4 Hz, 18H, P(*t*Bu)$_2$), 1.45 (m, 2H, TBDH(CH_2)), 1.41 (vt, J = 6.4 Hz, 18H, P(*t*Bu)$_2$), 1.24 (p, J = 5.9 Hz, 2H, TBDH(CH_2)). ^{13}C{^{1}H} NMR (100 MHz, C_6D_6): 167.61 (Cq, t, J_{P-C} = 8.2 Hz, $C_{Ar-ortho}$), 149.07 (Cq, s, TBDH), 132.82 (Cq, t, J_{P-C} = 5.2 Hz, $C_{Ar-ipso}$), 120.68 (CH, s, $C_{Ar-para}$), 102.85 (CH, t, J_{P-C} = 5.8 Hz, $C_{Ar-meta}$), 50.79 (CH_2, s, TBDH), 47.30 (CH_2, s, TBDH), 46.44 (CH_2, s, TBDH), 41.41 (CH, t, J_{P-C} = 10.8 Hz, P(*t*Bu)$_2$), 39.73 (CH, t, J_{P-C} = 10.4 Hz, P(*t*Bu)$_2$), 38.41 (CH_2, s, TBDH), 29.52 (CH_3, t, J_{P-C} = 3.9 Hz, P(*t*Bu)$_2$), 27.76 (CH_3, t, J_{P-C} = 4.1 Hz, P(*t*Bu)$_2$), 23.20 (CH_2, s, TBDH), 22.37 (CH_2, s, TBDH). ^{31}P{^{1}H} NMR (162 MHz, C_6D_6): 164.22. **8**: ^{1}H NMR (400 MHz, C_6D_6): 6.84 (m, 1H, *p*-H_{Ar}), 6.78 (m, 2H, *m*-H_{Ar}), 3.23 (t, J = 5.7 Hz, 2H, TBDH(CH_2)), 3.14 (t, J = 5.7 Hz, 2H,

TBDH(CH_2)), 2.70 (t, J = 5.7 Hz, 2H, TBDH(CH_2)), 2.66 (t, J = 5.7 Hz, 2H, TBDH(CH_2)), 1.66 (m, 4H, TBDH(CH_2)), 1.46 (vt, J = 6.7 Hz, 18H, P(tBu)$_2$), 1.33 (t, J = 6.7 Hz, 18H, P(tBu)$_2$), −24.71 (t, J = 15.5 Hz, 1H, IrH). $^{13}C\{^1H\}$ NMR (100 MHz, C_6D_6): 165.67 (Cq, t, $J_{P\text{-}C}$ = 6.0 Hz, $C_{Ar\text{-}ortho}$), 159.17 (Cq, s, TBDH), 122.94 (CH, s, $C_{Ar\text{-}para}$), 103.66 (CH, t, $J_{P\text{-}C}$ = 5.3 Hz, $C_{Ar\text{-}meta}$), 46.13 (CH_2, s, TBDH), 46.00 (CH_2, s, TBDH), 45.75 (CH_2, s, TBDH), 41.51 (CH_2, s, TBDH), 40.85 (CH, t, $J_{P\text{-}C}$ = 11.1 Hz, P(tBu)$_2$), 39.91 (CH, t, $J_{P\text{-}C}$ = 11.5 Hz, P(tBu)$_2$), 28.82 (CH_3, t, $J_{P\text{-}C}$ = 3.3 Hz, P(tBu)$_2$), 27.77 (CH_3, t, $J_{P\text{-}C}$ = 3.5 Hz, P(tBu)$_2$), 24.65 (CH_2, s, TBDH), 24.11 (CH_2, s, TBDH). $C_{Ar\text{-}ipso}$ is not observed. $^{31}P\{^1H\}$ NMR (162 MHz, C_6D_6): 150.89.

Results and discussion

Synthesis and characterization of the complexes

Recently, we have shown that [($^{t\text{Bu}}$POCOP)IrHCl] (**1**) is an efficient catalyst for the hydogenolysis of chlorosilanes in the presence of strong bases.[18] We therefore decided to investigate its behavior and that of related [($^{t\text{Bu}}$POCOP)IrHX] derivatives in the hydrogenolysis of the more reactive silyl triflates into hydrosilanes, in order to collect information on the species that are active during catalysis and the corresponding mechanism.

In a first experiment, **1** (1 mol%) was added to a mixture of Me_3SiOTf and NEt_3 in the 1:1.1 ratio under 1 bar H_2 in benzene. ^1H NMR monitoring of this mixture did not show any evolution after 48 h at r.t. However, when replacing **1** with the triflate analogue [($^{t\text{Bu}}$POCOP)IrH(OTf)] (**2**) or the dihydride derivative [($^{t\text{Bu}}$POCOP)IrH$_2$] (**3**), catalysis occurred and Me_3SiH was obtained in 83% yield after 3 h (Scheme 3). ^1H NMR monitoring evidenced the growth of a doublet at 0.00 ppm and a multiplet at 4.15 ppm, in the respective 9:1 integration ratio, characteristic of the gaseous Me_3SiH, as well as the presence of [($^{t\text{Bu}}$POCOP)Ir(H)$_2$(H$_2$)] (**4**) as the sole observable iridium complex (*vide infra*-Eqn 3). Surprisingly, using a stronger base, TBD, in the presence of 1 mol% of **3** did not lead to any turnover.

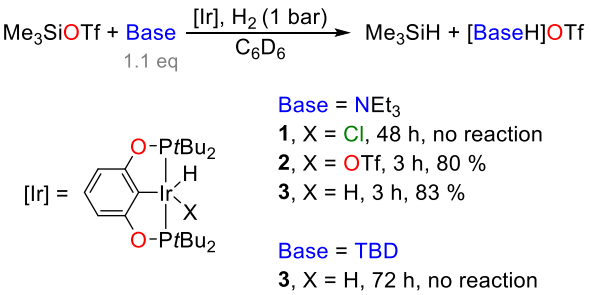

Scheme 3. First Catalytic experiments for the hydrogenolysis of silyl triflates

We tried to characterize and isolate the iridium complexes that might form during catalysis in order to highlight the role of the active species for both the hydride transfer and H_2 splitting. We thus synthesized the new complexes **2** and [($^{t\text{Bu}}$POCOP)IrH(NCMe)$_2$][OTf] (**5**) to gather information on the chemical behavior of the [($^{t\text{Bu}}$POCOP)IrH(X)] (X = Cl (**1**), OTf (**2**), H (**3**)) precursors when placed in presence of each of the reagents H_2, R_3SiOTf or the nitrogen base (NEt_3 or TBDH). The syntheses of the complexes are described in Scheme 4.

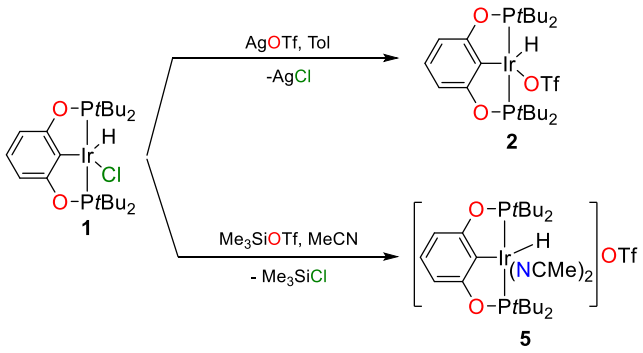

Scheme 4. Synthetic routes to the iridium pincer complexes 2 and 5.

Treatment of the chloro hydride precursor **1** with 1 equiv. of silver triflate (AgOTf) in toluene at r.t. overnight gave **2**, isolated after extraction from the silver salt as an orange powder in 96 % yield. Red-orange crystals of **2** were obtained by slow cooling of a saturated benzene solution heated under reflux. The ^1H NMR spectrum of **2** revealed a triplet for the Ir–H signal at δ = –42.9 ppm ($^2J_{P\text{-}H}$ = 10.8 Hz) (vs. δ = –40.9 ppm for **1** in C_6D_6).

The direct reaction of **1** with a slight excess of Me_3SiOTf in MeCN rapidly gave a pale yellow solution of the ion pair [($^{t\text{Bu}}$POCOP)IrH(MeCN)$_2$][OTf] (**5**), which was isolated in 78% yield after washing with pentane. Colorless crystalline blocks were grown from saturated solutions of **5** in MeCN or THF by slow diffusion of diethylether. Compound **5** exhibits in ^1H NMR (CD_3CN) a triplet at δ = –22.31 ppm ($^2J_{P\text{-}H}$ = 8.2 Hz) for the Ir–H signal which is shifted downfield in comparison to the resonance of the neutral counterpart **2**. Its related congener [($^{t\text{Bu}}$POCOP)IrH(MeCN)$_2$][B(C_6F_5)$_4$][56] exhibits an Ir–H resonance at δ = –20.9 ppm ($^2J_{P\text{-}H}$ = 14.7 Hz) close to that observed in **5**. Views of the crystal structures of [($^{t\text{Bu}}$POCOP)IrH(OTf)] (**2**) and its cationic derivative **5** are presented in Figure 1, together with selected bond lengths and angles. The Ir^{3+} ion in **2** is in a distorted square pyramidal environment, where the atoms P1, P2, C1 and O3A define the square basis (rms deviation 0.062 Å) with the hydrogen atom in apical position and the metal ion displaced by 0.1347(13) Å from the basis. Complex **5** comprises a six-coordinate Ir^{3+} ion in a distorted octahedral geometry with the two acetonitrile ligands in nearly perpendicular positions. One acetonitrile molecule faces the aromatic cycle while the other is *trans* to the hydride. In both complexes, the hydride is in the *cis* position compared to the C1 atom of the pincer ligand, a feature always observed in mono and dihydride iridium pincer complexes.[57] The slightly longer bond lengths in **5** certainly reflect the higher coordination number. These Ir–C1 distances of 1.990(3) Å and 2.024(4) Å in **2** and **5**, respectively, vary from 1.961(6) Å to 2.10(1) Å in a series of seventy-seven ^{R}POCOP iridium(I) and iridium(III) complexes reported in the Cambridge Structural Database (CSD, version 5.40)[57] and in which the Ir–P distances extend over the range 2.2408(9)–2.412(1) Å. The Ir–η^1-O(OTf) is classical for Ir–OTf complexes[58] and the Ir–N(acetonitrile) distances in **5** are comparable to those found in the two other reported iridium(III)-acetonitrile pincer complexes.[59,60] The Ir–H distances in **2** (1.52(4) Å) and **5** (1.46(4) Å) are quite identical to those in the complexes [($^{t\text{Bu}}$POCOP)IrHCl] (1.49(6) Å),[61] the cation [($^{t\text{Bu}}$POCOP)IrH(HSiEt$_3$)][B(C_6F_5)$_4$] (1.425(18) Å)[62] and the analogue of **4**, [($C_6H_2(CF_3)_3$POCOP)IrH$_2$(H$_2$)] (average 1.69 (3) Å).[63] Within the (^{R}POCOP)Ir(III) series, these Ir–H distances

scatter from 1.29(3) Å and 1.36(3) Å for [(tBu-POCOP)IrH$_2$(H$_2$PMes)] to 1.74(4) Å in [(tBu-POCOP)IrH$_2$(BH$_3$)].[64,65]

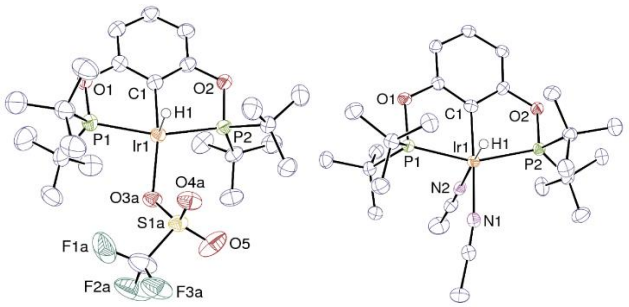

Figure 1. ORTEP views of **2** (left) and the cation [(tBu-POCOP)IrH(MeCN)$_2$]$^+$ in **5** (right). Displacement ellipsoids are drawn at the 50% probability level. Carbon-bound hydrogen atoms are omitted and only one position of the disordered triflate anion in **2** is shown. Selected bond lengths (Å) and angles (°). **2**: Ir1–C1 1.990(3), Ir1–O3a 2.211(3), Ir1–P1 2.2969(9), Ir1–P2 2.3147(9), Ir1–H1 1.52(4), C1–Ir1–O3A 167.74(14), P1–Ir1–P2 160.54(3), C1–Ir1–H1 88.5(16), C1–Ir1–P1 80.28(10), C1–Ir1–P2 80.33(10), O3a–Ir1–P1 93.56(9), O3a–Ir1–P2 105.17(9). **5**: Ir1–C1 2.024(4), Ir1–N1 2.101(3), Ir1–N2 2.159(3), Ir1–P1 2.3251(8), Ir1–P2 2.3308(9), Ir1–H1 1.46(4), C1–Ir1–N1 175.97(11), C1–Ir1–N2 97.44(13), P1–Ir1–P2 155.69(3), N1–Ir1–N2 85.34(12), C1–Ir1–P1 79.73(9), C1–Ir1–P2 79.11(9), N1–Ir1–P1 97.11(7), N1–Ir1–P2 103.42(8), N2–Ir1–P1 95.94(7), N2–Ir1–P2 98.53(7).

Because all neutral complexes **1**–**3** display good solubility in benzene, we then studied their reactivity in this solvent. Coordination of H_2 onto the complexes might be required for its further activation and use as a source of hydride. We first considered the behavior of the hydride species **1**–**3** under hydrogen (1 bar). If the formation of the dihydrogen complex **4** is well known from **3**,[66] coordination of H_2 was not detected on the more electron-deficient halide and triflate species for which the ^{1}H and ^{31}P NMR signals were left unchanged. (Eqn 1).

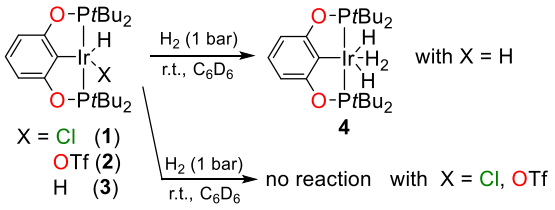

(1)

Hydrogenation processes catalyzed by metal complexes usually require the use of an anionic or neutral base in order to deprotonate the coordinated H_2.[67–70] Behavior of the hydride complexes **1**–**3** in presence of neutral nitrogen bases (NEt_3, TBDH (= 1,5,7-Triazabicyclo[4.4.0]dec-5-ene)) was thus investigated both under argon or dihydrogen. No change was observed by ^{1}H NMR spectroscopy when NEt_3 (1.1 equiv.) was added to each of the [(tBu-POCOP)IrH(X)] species in benzene under inert atmosphere (Eqn 2).

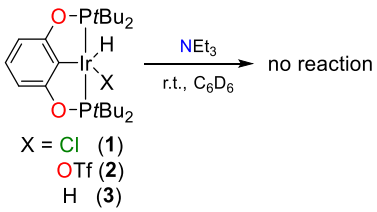

(2)

The absence of coordination of the triethylamine may be related to its steric congestion since the ammonia adduct [(tBuPCP)IrH(Cl)(NH$_3$)] (tBuPCP = C$_6$H$_3$(CH$_2$P^{t}Bu$_2$)$_2$) is known[71] and the two pincer ligands have similar steric hindrance. Some dihydride iridium pincers are also known to trap a variety of Lewis bases (NH_2NH_2, CO, phosphine).[64,72] No adduct of [(tBuPOCOP)IrH(Cl)] has been reported except the carbonyl derivative [(iPrPOCOP)IrH(Cl)(CO)].[73] Importance of the steric effects in the coordination number of iridium complexes and on the stability of iridium(I) versus iridium(III) compounds has already been clearly underlined.[73] Replacing argon with 1 bar H_2 on the [(tBuPOCOP)IrH(X)]:NEt_3 (1:1.1 ratio) mixture gave no reaction with **1** while **4** is quantitatively obtained from **2** and **3** (with the concomitant release of [HNEt$_3$]OTf in the case of **2**) (Eqn 3).

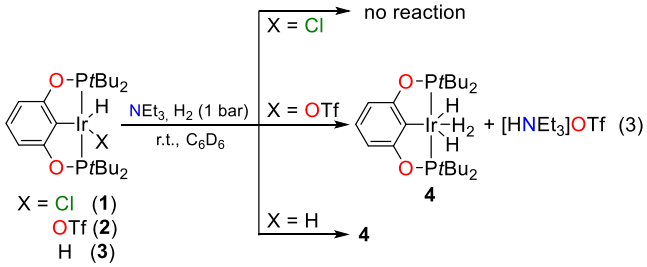

(3)

In addition to its steric congestion, the Brønstedt basicity[74,75] of the base plays also an important role in its interaction with the metal center and/or its ability to deprotonate dihydrogen or hydride ligands. Guanidine TBDH is a stronger base (pKa = 26.0 in MeCN) than NEt_3 (pKa = 18.8 in MeCN) and is used in a variety of base-mediated organic transformations and catalytic processes.[76–79]

Treatment of dihydride **3** with 1 equiv. TBDH afforded quantitatively the adduct [(tBuPOCOP)IrH$_2$(TBDH)] (**6**) (Eqn 4). The latter is present as two isomers in solution (cis and trans). This results in two ^{31}P{^{1}H} NMR signals superimposed at 168.0 ppm as well as relatively complex hydridic signals : two triplets at δ = −9.05 and 9.41 (J_{P-H} = 14.5 and 15.9 Hz respectively) for the trans isomer and two triplets of doublets at δ = −9.16 and −9.59 (J_{P-H} = 14.7 and 17.7 Hz and J_{H-H} = 11.4 Hz) for the cis isomer. This cis/trans isomerism has been reported for the closely related carbonyl complexes by Goldberg, Heinekey, *et al.*[71]

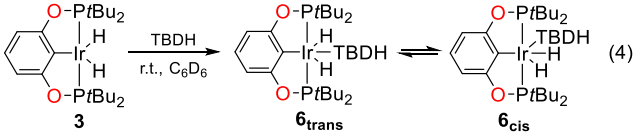

(4)

In contrast, the reaction of [(tBuPOCOP)IrH(X)] (X = Cl, OTf) with 2 equiv. of TBDH in benzene led to the formation of [(tBu-POCOP)Ir(TBDH)]. NMR spectroscopy evidenced formation of a mixture of **7** and its iridium(III) counterpart [(tBu-POCOP)IrH(TBD)] (**8**) in the ratio 60:40 from the chloro hydride **1** or from the triflato hydride **2**, respectively, at room temperature (Eqn 5).

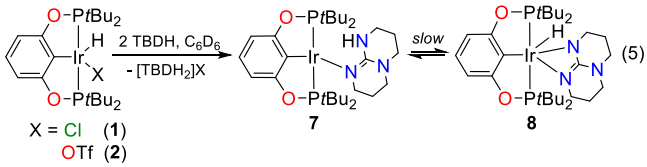

(5)

Reaction of 2 equiv. TBDH with **1** or **2** or 1 equiv. [TBD]K and **1** in benzene led to the same distribution of complexes **7** and **8** (60:40 respectively). Complexes **7** and **8** are likely the different

redox forms of the same product that are in slow equilibrium at the NMR timescale. Such an equilibrium was already observed on iridium pincer complexes, such as [($^{t\text{Bu}}$PCP)Ir] which reacted with the amine NH_2(*m*-xylyl) to give [($^{t\text{Bu}}$PCP)IrH(NH(*m*-xylyl))].[80] ^{1}H and ^{31}P{^{1}H} NMR investigations at various temperatures showed slight variations in the **7**:**8** ratio, which does not give clear evidence for such an equilibrium. We expected that formation of this mixture would be influenced in the presence of a coordinating solvent. Indeed, when heated in acetonitrile, this mixture gave back the sole iridium(I) species [($^{t\text{Bu}}$POCOP)Ir(NCMe)] **9** (Eqn 6), which has already been reported[81] when reacting NaO*t*Bu with **1** in acetonitrile.

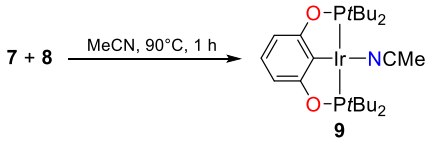

(6)

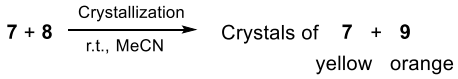

(7)

Crystallization by slow cooling of a saturated acetonitrile solution of **7** and **8** afforded concomitantly large pale-yellow blocks of [($^{t\text{Bu}}$POCOP)Ir(TBDH)] (**7**) and orange crystals of **9** (Eqn 7). ORTEP views of their crystal structures are presented in Figure 2 with selected bond lengths and angles. The iridium(I) metal centers in **7** and **9** are in a square-planar environment and complex **9** has mirror symmetry, atoms Ir1, C1, and N1 being located on the mirror plane. In order to minimize steric interactions, the TBDH ligand in **7** adopts a position perpendicular to the plane containing the Ir1, P1, P2, C1 and N1 atoms as it was found in the closely similar complex [($^{\text{CF}3}$PCP)Ir(DBU)].[82] The Ir–N distance in **7** (2.192(3) Å) is higher than in **9** (2.043(3) Å). Since TBDH is a stronger Lewis base than acetonitrile, the longer Ir–N bond length in **7** may indicate a higher steric strain hindering its coordination. This could explain the displacement of TBDH ligand with acetonitrile.

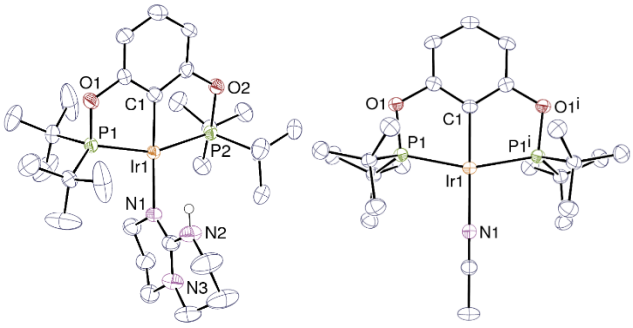

Figure 2. ORTEP views of complexes **7** (left) and **9** (right). Displacement ellipsoids are drawn at the 50% probability level and carbon-bound hydrogen atoms are omitted. Symmetry code: i = x, y, 1/2 – z. Selected bond lengths (Å) and angles (°). **7**: Ir1–C1 2.015(4), Ir1–N1 2.192(3), Ir1–P1 2.2698(10), Ir1–P2 2.2866(11), C1–Ir1–N1 175.45(15), P1–Ir1–P2 156.59(4), C1–Ir1–P1 79.03(12), C1–Ir1–P2 79.08(13), N1–Ir1–P1 100.83(10), N1–Ir1–P2 101.66(10). **9**: Ir1–C1 2.008(4), Ir1–N1 2.043(3), Ir1–P1 2.2479(7), C1–Ir1–N1 178.77(13), P1–Ir1–P1^{i} 159.11(4), C1–Ir1–P1 79.556(19), N1–Ir1–P1 100.436(19).

If such a reductive dehydrochlorination of iridium(III) to iridium(I) compounds in the presence of strong anionic bases (KO*t*Bu, LiEt$_3$BH, and KH) is expected,[83] reduction with neutral bases is rather uncommon. In addition to our work, a single example could be found with neutral organic bases that could generate an iridium(I) complex from iridium(III) chloro hydride precursor.[82]

Note that under 1 bar of H_2, the mixture of **7** and **8** is entirely converted into the dihydride iridium(III) complex $\mathbf{6_{cis}}$. Formation of this latter may result either from H_2 oxidative addition on the iridium(I) complex **7** or the deprotonation of coordinated H_2 on **8** by its anionic TBD ligand (Eqn 8).

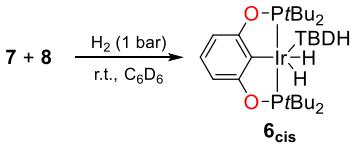

(8)

It is interesting to note that the HOMO-1 and LUMO of **7** show a strong overlap between the dz² orbital centered on the iridium(I) ion and the σ^*_{N-H} orbital of the TBDH ligand (Figure 3). This destabilizing interaction favors intramolecular oxidative addition of **7** into **8**.

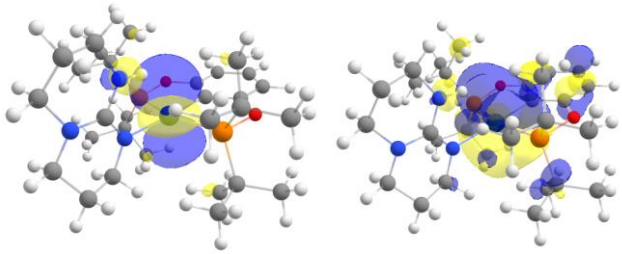

Figure 3. HOMO-1 (left) and LUMO (right) of **7**

The reactivity of metal hydride complexes **1**–**3** and **4** was then considered with Me_3SiOTf in benzene in order to probe their capacity at hydride transfer to form hydrosilanes. No reaction was observed with any of the complexes in presence of 1 equiv. or excess Me_3SiOTf, either at room temperature or at 90°C (Eqn 9). Similarly, the hydrogen adduct **4** was found to be inert under an H_2 atmosphere. Hydride transfer is therefore not favored with these iridium(III) complexes. It is in contrast to the ruthenium(II) complex [(HN{$CH_2CH_2P(^iPr)_2$}$_2$)Ru(H)$_2$(CO)] which readily transfers a hydride to Me_3SiX (X = Cl, OTf) to give Me_3SiH and [(HN{$CH_2CH_2P(^iPr)_2$}$_2$))RuH(X)(CO)] almost quantitatively in benzene.[66] The Si–OTf to Si–H reaction that we wished to perform is actually thermodynamically unfavorable, since the reverse reaction easily took place in benzene (Eqn 10). Indeed, in presence of 5 equiv. Et_3SiH, [($^{t\text{Bu}}$POCOP)IrH(OTf)] was quantitatively transformed into dihydride complex **3** within 18 h at room temperature. Previously, Brookhart *et al.* reported the conversion of chloro hydride **1** into dihydride **3** with an excess of Et_3SiH but only when the ion pair [($^{t\text{Bu}}$POCOP)IrH(acetone)][B(C_6F_5)$_4$] was added as catalyst.[56] We have also shown in a recent study[18] that the hydride transfer on silyl chloride required a more reactive hydride species such as anionic complex **10** which readily transfers one of its hydride to Me_3SiCl (Eqn 11). However, such active species could only be generated in the presence of very strong bases such as Verkade's base ($^{i\text{Pr}}$VB = 2,8,9-Triisopropyl-2,5,8,9-tetraaza-1-phosphabicyclo[3.3.3]undecane) or phosaphazene.

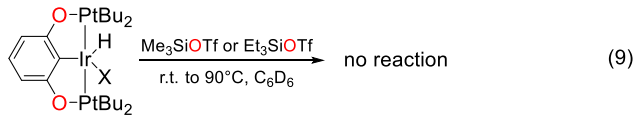

(9)

X = H (**3**), H(H$_2$) (**4**)
Cl (**1**), OTf (**2**)

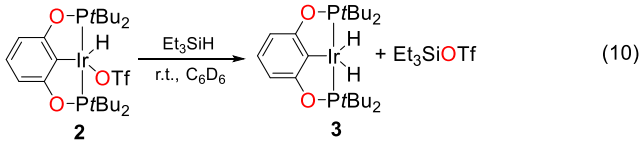

2 **3** (10)

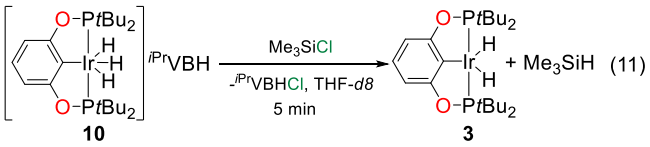

10 **3** (11)

The weak NEt$_3$ base does not induce formation of an anionic [POCOP)IrH$_3$]$^-$ species (Eqn 3) and the above results would suggest that **3** is most likely the active species in hydride transfer. Although the [(^{tBu}POCOP)IrH(X)] complexes proved unable to reduce a silyl triflate into an hydrosilane (Eqn 9), it does not necessarily prevent a catalytic turnover as the unfavorable thermodynamics of the hydride transfer might be counterbalanced by the overall favorable hydrogenolysis reaction.

Catalytic hydrogenolysis of silyl triflates

Complexes **1**, **2**, **3**, **7** and **8** have been tested in benzene for the hydrogenolysis of silyl triflates into silanes under 1 bar of H$_2$ at room temperature and in the presence of triethylamine. The chloro hydride complex **1** did not show any activity, even after 48 h (Table 1, Entry 1). Complexes **2** and **3** were expected to behave similarly, since they can both evolve to **4** in the presence of NEt$_3$ and H$_2$. Effectively, both **2** and **3** displayed a catalytic activity and Me$_3$SiH was obtained in 80 and 83% yield respectively, after 3 h (Table 1, Entries 2-3). Complexes **7** and **8** are also able to catalyze the reaction, yielding 78% of Me$_3$SiH after 3 h (Table 1, Entry 4). Replacing the base NEt$_3$ with TBDH was deleterious to the catalysis, and Me$_3$SiH was not detected when using **3**, even after 72 h (Table 1, Entry 5). Complex **3** is also efficient in the catalytic hydrogenolysis of Et$_3$SiOTf and Ph$_3$SiOTf but these reactions required longer reaction times: the corresponding hydrosilanes were formed in 86% and 55% yields after 8 h and 300 h, respectively (Table 1, Entries 6 and 7). The detrimental steric influence of large R groups on R$_3$SiX has already been noticed by the groups of Shimada and Schneider.[16,17]

Table 1. Catalytic hydrogenolysis of silyl triflates[a]

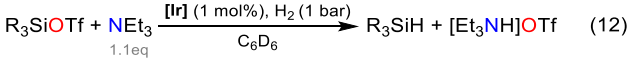

(12)

Entry	[Ir]	Substrate	Base	Conv[b] (%)	Product (yield[b])	Time (h)
1	**1**	Me$_3$SiOTf	NEt$_3$	0	-	48
2	**2**	Me$_3$SiOTf	NEt$_3$	83	Me$_3$SiH (80%)	3
3	**3**	Me$_3$SiOTf	NEt$_3$	85	Me$_3$SiH (83%)	3
4	**7/8**	Me$_3$SiOTf	NEt$_3$	80	Me$_3$SiH (78%)	3
5[c]	**3**	Me$_3$SiOTf	TBDH	0	-	72
6	**3**	Et$_3$SiOTf	NEt$_3$	88	Et$_3$SiH (83%) (82%)[d]	8
7	**3**	Ph$_3$SiOTf	NEt$_3$	60	Ph$_3$SiH (55%) (59%) [d]	300

[a] General conditions: 0.1 mmol of substrate, 1 µmol of catalyst, 1 bar of H$_2$, 0.5 mL of C$_6$D$_6$, room temperature.[b] Conversions/yields were determined by ^{1}H NMR integration of all signals in the R$_3$Si region around 0 ppm versus an internal standard (1,3,5-trimethylbenzene).[c] r.t. to 90°C. [d]GC-MS yield (see SI, 2.4).

Complex **3** is active for the conversion of Me$_3$SiOTf to Me$_3$SiH that is obtained in 80% yield after 3 h. This result can be compared with that of the group of Schneider, who reported similar yields for the same reaction catalyzed by the the bifunctional Ru(II)-MACHO complex [(HN{CH$_2$CH$_2$P(^{i}Pr)$_2$}$_2$)Ru(H)$_2$(CO)] (1 mol%) but after 18 h reaction and under 4 bar of H$_2$.[17] A surprising result is the total shutdown of the catalysis when a stronger base, TBDH, is used instead of NEt$_3$. The Gibbs free energies of both reactions was computed, and the formation of Me$_3$SiH + [TBDH$_2$]OTf appears to be much more exergonic than that with [NEt$_3$H]OTf (ΔG = –14.1 vs. –0.4 kcal.mol^{-1}). While the catalysis should thermodynamically be more favorable with TBDH, the rapid reaction of TBDH with Me$_3$SiOTf to produce [Me$_3$Si–TBDH]OTf (ΔG = –12.1 kcal.mol^{-1}) is detrimental. Indeed, the latter species precipitates and is inert even at higher temperatures (up to 90 °C). This side reaction explains the absence of catalytic activity with TBDH. In addition, a similar adduct [Me$_3$Si–NEt$_3$]OTf was formed when the reaction with NEt$_3$ was performed in acetonitrile and the expected hydrosilane was not obtained (See ESI, Section 1.2.3). This is in line with our recent results in the hydrogenolysis of chlorosilanes.[18] The low exergonicity of the reaction with NEt$_3$ (ΔG = –0.4 kcal.mol^{-1}) should lead to an equilibrium, but the poor miscibility of the ionic liquid [HNEt$_3$]OTf leads to a phase separation that drives the reaction to the formation of Me$_3$SiH (See ESI, Section 1.2.4).

Density functional theory calculations were performed to obtain further insight on the hydrogenolysis mechanism by these iridium pincer complexes (Scheme 5). The mechanistic route highlights the facile interconversion between complexes **3** and **4** (0 and –0.4 kcal.mol^{-1} respectively) which can proceed in ambient conditions through TS$_{3\text{-}4}$ at +11.3 kcal.mol^{-1}. Both complexes might be the active species. Complex **4** is immediately obtained by hydrogenation of **3** and is observed during the catalysis and at its end (Eqn 2). The hydride transfer from **3** or **4** to Me$_3$SiOTf is barrierless and leads to the formation of an intermediate at 10.9 kcal.mol^{-1} (**I1**) or at 18.0 kcal.mol^{-1} respectively (see SI Fig. S28). It seems however unlikely that **4** is the active species with such an energetic gap (7.1 kcal.mol^{-1}) between these two intermediates and therefore **4** would be an off-cycle species. Formation of the triflato hydride complex **2** with release of Me$_3$SiH from **I1** is exergonic ($\Delta\Delta G°$ = –10.4 kcal.mol^{-1}) with a high energetic barrier involving TS$_{I1\text{-}2}$ ($\Delta G°$ = +21.5 kcal.mol^{-1}).

Coordination of H$_2$ onto **2** proceeds through **TS$_{2\text{-}I2}$** ($\Delta G°$ = +8.0 kcal.mol^{-1}) giving **I2** ($\Delta G°$ = +6.8 kcal.mol^{-1}). Base-assisted splitting of H$_2$ relies on a high energetic barrier of +24.9 kcal.mol^{-1} (TS$_{I3\text{-}I4}$) which leads to the ion pair **I4** ($\Delta G°$ = +17.9 kcal.mol^{-1}). Finally, regeneration of the dihydride **3** is facile and proceed through **TS$_{I4\text{-}3}$** ($\Delta G°$ = +18.5 kcal.mol^{-1}) with the release of [HNEt$_3$]OTf. For this mechanistic route (purple + orange lines), the energetic span of 25.3 kcal.mol^{-1} is defined by **TS$_{I2\text{-}I4}$** and **4**, and is slightly higher (by 3-4 kcal.mol^{-1}) than expected from the experimental conditions at room temperature (Eqn 12). This relatively high value may be related to the difficult approach of the base toward the complex due to steric hindrance. Formation of the iridium(I) adduct [(^{tBu}-

POCOP)Ir(OTf)][HNEt$_3$] (**I3**) (23.7 kcal.mol^{-1}) by deprotonation of **2** with NEt$_3$ was considered. Its formation reveals a high energetic barrier ($\Delta G°$ = 32.2 kcal.mol^{-1} for **TS$_{2\text{-}I3}$**) that makes it unlikely. DFT calculations suggest that the splitting of H_2 would result from iridium(III) rather than iridium(I) species. This is in agreement with the experiment where no iridium(I) intermediate has been evidenced by reacting **1**, **2** or **3** with NEt$_3$ (Eqn 4).

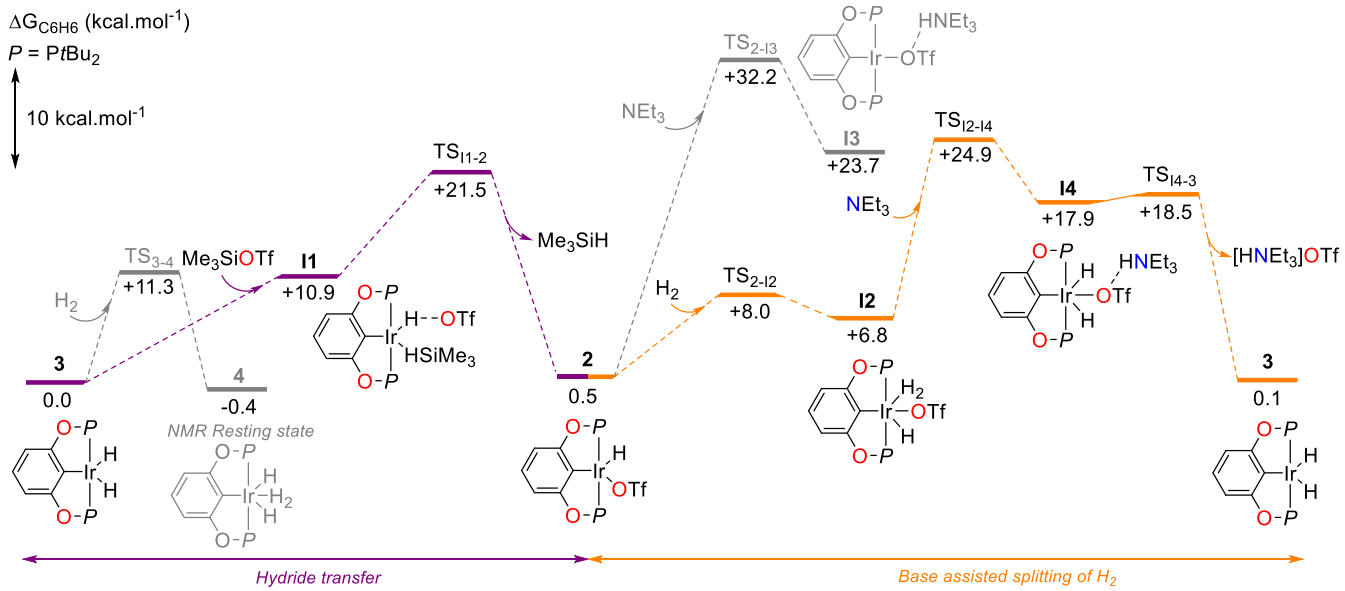

Scheme 5. Computed pathway for the mechanism of the catalytic transformation of Me_3SiOTf into Me_3SiH by 3. Values given are Gibbs free energies in kcal.mol^{-1} with respect to 3 + Me_3SiOTf (0.0). Computations parameters: Gaussian 16 Rev. C01, PBE0-D3/Def2-TZVP (Ir), 6-311+G(d,p) (Si, mobile H), 6-31G(d) (other atoms), SMD (Solvent: benzene).

Conclusion

We showed that iridium(III) complexes **2** and **3**, as well as iridium(I) TBDH adduct **7**, are able to catalyze the hydrogenolysis of silyl triflates R_3SiOTf (R = Me, Et, Ph) in the presence of the NEt$_3$. The reaction proceeds under mild conditions (r.t.,1 bar H_2) and affords the corresponding hydrosilanes with good yields and selectivity. The reaction works well in benzene in the presence of the base NEt$_3$ but not with the guanidine TBDH which reacts rapidly with silyl triflates (R_3SiOTf) to give the insoluble and deactivated species [R_3Si-TBDH]OTf. The yield and selectivity in hydrosilanes are similar to those afforded by other iridium(III) catalysts, but the reaction conditions are milder (1 bar H_2 *vs* 4 bar). The reaction is however much faster (TOF of 28 h^{-1}) than with any other reported catalysts (TOF of 0.2 and 18 h^{-1}).[16,17] To gain insight into the mechanism, the chemical reactivity of complexes **1**–**3** with the reagents involved in the catalysis has been scrutinized. Some iridium complexes have been isolated or experimentally characterized and these studies revealed that iridium(I) complexes may form, depending on the nature of the base. However, the involvement of catalytically active iridium(I) species in hydrogenolysis is dismissed by DFT calculations which revealed that only iridium(III) complexes are efficient *via* σ-bond metathesis steps and hydride transfers.

AUTHOR INFORMATION

Corresponding Author

* E-mail: thibault.cantat@cea.fr; Fax: +33 1 6908 6640; Tel: +33 1 6908 4338

† Université Paris-Saclay, CEA, CNRS, NIMBE, 91191, Gif-sur-Yvette, France.

Author Contributions

The manuscript was written with contributions of all authors. All authors have given approval to the final version of the manuscript.

Funding Sources

For financial support of this work, we acknowledge CEA, CNRS, the University Paris-Saclay, CINES (HPC Computing time on Occigen, grant no. A0080806494) and the European Research Council (ERC Consolidator Grant Agreement no. 818260). T.C. thanks the Fondation Louis D.–Institut de France for its major support.

ASSOCIATED CONTENT

The following files are available free of charge. Supplementary equations, detailed descriptions of experimental methods, kinetic and mechanism studies are provided in the Supporting Information.

Accession Codes

CCDC 2077245–2077248 contain the supplementary crystallographic data for this paper. These data can be obtained free of charge via www.ccdc.cam.ac.uk/data_request/cif, or by emailing data_request@ccdc.cam.ac.uk, or by contacting The Cambridge Crystallographic Data Centre, 12 Union Road, Cambridge CB2 1EZ, UK; fax: +44 1223 336033.

REFERENCES

(1) Simmler, W. Silicon Compounds, Inorganic. In *Ullmann's Encyclopedia of Industrial Chemistry*; Wiley, **2000**, pp 616–635.

(2) Marciniec, B. Functionalisation and Cross-Linking of Organosilicon Polymers. In *Hydrosilylation*, Springer, **2009**, pp 159–189.

(3) Rösch, L.; John, P.; Reitmeier, R. Silicon Compounds, Organic. In *Ullmann's Encyclopedia of Industrial Chemistry*; Wiley, **2000**, pp 664–669.

(4) Cheng, C.; Hartwig, J. F. Catalytic Silylation of Unactivated C–H Bonds. *Chem. Rev.* **2015**, *115*, 8946–8975.

(5) Li, H.; Misal Castro, L. C.; Zheng, J.; Roisnel, T.; Dorcet, V.; Sortais, J.-B.; Darcel, C. Selective Reduction of Esters to Aldehydes under the Catalysis of Well-Defined NHC-Iron Complexes. *Angew. Chem. Int. Ed.* **2013**, *52*, 8045–8049.

(6) Hosokawa, S.; Toya, M.; Noda, A.; Morita, M.; Ogawa, T.; Motoyama, Y. Catalytic Silane-Reduction of Carboxylic Esters and Lactones: Selective Synthetic Methods to Aldehydes, Lactols, and Ethers via Silyl Acetal Intermediates. *ChemistrySelect* **2018**, *3*, 2958–2961.

(7) Das, S.; Addis, D.; Junge, K.; Beller, M. Zinc-Catalyzed Chemoselective Reduction of Tertiary and Secondary Amides to Amines. *Chem. Eur. J.* **2011**, *17*, 12186–12192.

(8) Pesti, J.; Larson, G. L. Tetramethyldisiloxane: A Practical Organosilane Reducing Agent. *Org. Process Res. Dev.* **2016**, *20*, 1164–1181.

(9) Riduan, S. N.; Zhang, Y.; Ying, J. Y. Conversion of Carbon Dioxide into Methanol with Silanes over N-Heterocyclic Carbene Catalysts. *Angew. Chem. Int. Ed.* **2009**, *48*, 3322–3325.

(10) Monsigny, L.; Feghali, E.; Berthet, J.-C.; Cantat, T. Efficient Reductive Depolymerization of Hardwood and Softwood Lignins with Brookhart's Iridium(III) Catalyst and Hydrosilanes. *Green Chem.* **2018**, *20*, 1981–1986.

(11) Monsigny, L.; Berthet, J.-C.; Cantat, T. Depolymerization of Waste Plastics to Monomers and Chemicals Using a Hydrosilylation Strategy Facilitated by Brookhart's Iridium(III) Catalyst. *ACS Sustain. Chem. Eng.* **2018**, *6*, 10481–10488.

(12) Kalchauer, W.; Pachaly, B. *Handbook of Heterogenous Catalysis*; Wiley-VCH Verlag GmbH, **2008**, pp 2635–2647.

(13) Nishibayashi, Y.; Takei, I.; Hidai, M. Novel Catalytic Hydrogenolysis of Trimethylsilyl Enol Ethers by the Use of an Acidic Ruthenium Dihydrogen Complex. **1999**, *38*, 3047–3050.

(14) Takei, I.; Nishibayashi, Y.; Ishii, Y.; Mizobe, Y.; Uemura, S.; Hidai, M. Novel Catalytic Hydrogenolysis of Silyl Enol Ethers by the Use of Acidic Ruthenium Dihydrogen Complexes. *J. Organomet. Chem.* **2003**, *679*, 32–42.

(15) Tsushima, D.; Igarashi, M.; Sato, K.; Shimada, S. Ir-Catalyzed Hydrogenolysis Reaction of Silyl Triflates and Halides with H_2. *Chem. Lett.* **2017**, *46*, 1532–1534.

(16) Beppu, T.; Sakamoto, K.; Nakajima, Y.; Matsumoto, K.; Sato, K.; Shimada, S. Hydrosilane Synthesis via Catalytic Hydrogenolysis of Halosilanes Using a Metal-Ligand Bifunctional Iridium Catalyst. *J. Organomet. Chem.* **2018**, *869*, 75–80.

(17) Glüer, A.; Schweizer, J. I.; Karaca, U. S.; Würtele, C.; Diefenbach, M.; Holthausen, M. C.; Schneider, S. Hydrosilane Synthesis by Catalytic Hydrogenolysis of Chlorosilanes and Silyl Triflates. *Inorg. Chem.* **2018**, *57*, 13822–13828.

(18) Gabriel Durin; Berthet, J.-C.; Nicolas, E.; Cantat, T. Unlocking the Catalytic Hydrogenolysis of Chlorosilanes into Hydrosilanes with Superbases. *ChemRxiv* **2021**. https://doi.org/10.26434/chemrxiv.14356154.

(19) Jia, J.; Seitz, L. C.; Benck, J. D.; Huo, Y.; Chen, Y.; Ng, J. W. D.; Bilir, T.; Harris, J. S.; Jaramillo, T. F. Solar Water Splitting by Photovoltaic-Electrolysis with a Solar-to-Hydrogen Efficiency over 30%. *Nat. Commun.* **2016**, *7*, 13237.

(20) Hisatomi, T.; Domen, K. Reaction Systems for Solar Hydrogen Production via Water Splitting with Particulate Semiconductor Photocatalysts. *Nat. Catal.* **2019**, *2*, 387–399.

(21) Clarke, Z. E.; Maragh, P. T.; Dasgupta, T. P.; Gusev, D. G.; Lough, A. J.; Abdur-Rashid, K. A Family of Active Iridium Catalysts for Transfer Hydrogenation of Ketones. *Organometallics* **2006**, *25*, 4113–4117.

(22) Tanaka, R.; Yamashita, M.; Nozaki, K. Catalytic Hydrogenation of Carbon Dioxide Using Ir(III)−Pincer Complexes. *J. Am. Chem. Soc.* **2009**, *131*, 14168–14169.

(23) Park, S.; Brookhart, M. Hydrosilylation of Carbonyl-Containing Substrates Catalyzed by an Electrophilic η^1-Silane Iridium(III) Complex. *Organometallics* **2010**, *29*, 6057–6064.

(24) Göttker-Schnetmann, I.; White, P.; Brookhart, M. Iridium Bis(Phosphinite) *p* -XPCP Pincer Complexes: Highly Active Catalysts for the Transfer Dehydrogenation of Alkanes. *J. Am. Chem. Soc.* **2004**, *126*, 1804–1811.

(25) Hooft, R. W. W. COLLECT, Nonius BV Delft, The Netherlands, **1998**.

(26) Otwinowski, Z.; Minor, W. [20] Processing of X-Ray Diffraction Data Collected in Oscillation Mode. In *Methods in Enzymology*; Elsevier, 1997; Vol. 276, pp 307–326.

(27) Sheldrick, G. M. *SHELXT* – Integrated Space-Group and Crystal-Structure Determination. *Acta Crystallogr. Sect. Found. Adv.* **2015**, *71*, 3–8.

(28) Sheldrick, G. M. Crystal Structure Refinement with *SHELXL*. *Acta Crystallogr. Sect. C Struct. Chem.* **2015**, *71*, 3–8.

(29) Farrugia, L. J. *WinGX* and *ORTEP for Windows* : An Update. *J. Appl. Crystallogr.* **2012**, *45*, 849–854.

(30) Gaussian 16 Rev C.01, M. J. Frisch, G. W. Trucks, H. B. Schlegel, G. E. Scuseria, M. A. Robb, J. R. Cheeseman, G. Scalmani, V. Barone, G. A. Petersson, H. Nakatsuji, X. Li, M. Caricato, A. V. Marenich, J. Bloino, B. G. Janesko, R. Gomperts, B. Mennucci, H. P. Hratchian, J. V. Ortiz, A. F. Izmaylov, J. L. Sonnenberg, D. Williams-Young, F. Ding, F. Lipparini, F. Egidi, J. Goings, B. Peng, A. Petrone, T. Henderson, D. Ranasinghe, V. G. Zakrzewski, J. Gao, N. Rega, G. Zheng, W. Liang, M. Hada, M. Ehara, K. Toyota, R. Fukuda, J. Hasegawa, M. Ishida, T. Nakajima, Y. Honda, O. Kitao, H. Nakai, T. Vreven, K. Throssell, J. A. Montgomery, Jr., J. E. Peralta, F. Ogliaro, M. J. Bearpark, J. J. Heyd, E. N. Brothers, K. N. Kudin, V. N. Staroverov, T. A. Keith, R. Kobayashi, J. Normand, K. Raghavachari, A. P. Rendell, J. C. Burant, S. S. Iyengar, J. Tomasi, M. Cossi, J. M. Millam, M. Klene, C. Adamo, R. Cammi, J. W. Ochterski, R. L. Martin, K. Morokuma, O. Farkas, J. B. Foresman, and D. J. Fox, Gaussian, Inc., Wallingford CT, **2016**.

(31) Adamo, C.; Barone, V. Toward Reliable Density Functional Methods without Adjustable Parameters: The PBE0 Model. *J. Chem. Phys.* **1999**, *110*, 6158–6170.

(32) Grimme, S.; Antony, J.; Ehrlich, S.; Krieg, H. A Consistent and Accurate Ab Initio Parametrization of Density Functional Dispersion Correction (DFT-D) for the 94 Elements H-Pu. *J. Chem. Phys.* **2010**, *132*, 154104.

(33) Weigend, F. Accurate Coulomb-Fitting Basis Sets for H to Rn. *Phys. Chem. Chem. Phys.* **2006**, *8*, 1057.

(34) Weigend, F.; Ahlrichs, R. Balanced Basis Sets of Split Valence, Triple Zeta Valence and Quadruple Zeta Valence Quality for H to Rn: Design and Assessment of Accuracy. *Phys. Chem. Chem. Phys.* **2005**, *7*, 3297.

(35) Schäfer, A.; Horn, H.; Ahlrichs, R. Fully Optimized Contracted Gaussian Basis Sets for Atoms Li to Kr. *J. Chem. Phys.* **1992**, *97*, 2571–2577.

(36) Schäfer, A.; Huber, C.; Ahlrichs, R. Fully Optimized Contracted Gaussian Basis Sets of Triple Zeta Valence Quality for Atoms Li to Kr. *J. Chem. Phys.* **1994**, *100*, 5829–5835.

(37) Binning Jr., R. C.; Curtiss, L. A. Compact Contracted Basis Sets for Third-row Atoms: Ga–Kr. *J. Comput. Chem.* **1990**, *11*, 1206-1216.

(38) McLean, A. D.; Chandler, G. S. Contracted Gaussian Basis Sets for Molecular Calculations. I. Second Row Atoms, Z=11–18. *J. Chem. Phys.* **1980**, *72*, 5639–5648.

(39) McGrath, M. P.; Radom, L. Extension of Gaussian-1 (G1) Theory to Bromine-containing Molecules. *J. Chem. Phys.* **1991**, *94*, 511–516.

(40) Curtiss, L. A.; McGrath, M. P.; Blaudeau, J.-P.; Davis, N. E.; Binning, R. C.; Radom, L. Extension of Gaussian-2

Theory to Molecules Containing Third-row Atoms Ga–Kr. *J Chem Phys* **1995**, *103*, 11.

(41) Wachters, A. J. H. Gaussian Basis Set for Molecular Wavefunctions Containing Third-Row Atoms. *J. Chem. Phys.* **1970**, *52*, 1033–1036.

(42) Hay, P. J. Gaussian Basis Sets for Molecular Calculations. The Representation of 3d Orbitals in Transition-metal Atoms. **1977**, *66*, 9.

(43) Raghavachari, K.; Trucks, G. W. Highly Correlated Systems. Excitation Energies of First Row Transition Metals Sc–Cu. **1989**, *91*, 5.

(44) Krishnan, R.; Binkley, J. S.; Seeger, R.; Pople, J. A. Self-consistent Molecular Orbital Methods. XX. A Basis Set for Correlated Wave Functions. *J. Chem. Phys.* **1980**, *72*, 650–654.

(45) Rassolov, V. A.; Pople, J. A.; Ratner, M. A.; Windus, T. L. 6-31G * Basis Set for Atoms K through Zn. *J. Chem. Phys.* **1998**, *109*, 1223–1229.

(46) Rassolov, V. A.; Ratner, M. A.; Pople, J. A.; Redfern, P. C.; Curtiss, L. A. 6-31G* Basis Set for Third-Row Atoms. *J. Comput. Chem.* **2001**, *22*, 976–984.

(47) Hariharan, P. C.; Pople, J. A. Accuracy of AHn Equilibrium Geometries by Single Determinant Molecular Orbital Theory. *Mol. Phys.* **1974**, *27*, 209–214.

(48) Binning, R. C.; Curtiss, L. A. Compact Contracted Basis Sets for Third-Row Atoms: Ga-Kr. *J. Comput. Chem.* **1990**, *11*, 1206–1216.

(49) Blaudeau, J.-P.; McGrath, M. P.; Curtiss, L. A.; Radom, L. Extension of Gaussian-2 (G2) Theory to Molecules Containing Third-Row Atoms K and Ca. *J. Chem. Phys.* **1997**, *107*, 5016–5021.

(50) Francl, M. M.; Pietro, W. J.; Hehre, W. J.; Binkley, J. S.; Gordon, M. S.; DeFrees, D. J.; Pople, J. A. Self-consistent Molecular Orbital Methods. XXIII. A Polarization-type Basis Set for Second-row Elements. *J. Chem. Phys.* **1982**, *77*, 3654–3665.

(51) Ditchfield, R.; Hehre, W. J.; Pople, J. A. Self-Consistent Molecular-Orbital Methods. IX. An Extended Gaussian-Type Basis for Molecular-Orbital Studies of Organic Molecules. *J. Chem. Phys.* **1971**, *54*, 724–728.

(52) Hehre, W. J.; Ditchfield, R.; Pople, J. A. Self—Consistent Molecular Orbital Methods. XII. Further Extensions of Gaussian—Type Basis Sets for Use in Molecular Orbital Studies of Organic Molecules. *J. Chem. Phys.* **1972**, *56*, 2257–2261.

(53) Hariharan, P. C.; Pople, J. A. The Influence of Polarization Functions on Molecular Orbital Hydrogenation Energies. *Theor. Chim. Acta* **1973**, *28*, 213–222.

(54) Gordon, M. S. The Isomers of Silacyclopropane. *Chem. Phys. Lett.* **1980**, *76*, 163–168.

(55) Marenich, A. V.; Cramer, C. J.; Truhlar, D. G. Universal Solvation Model Based on Solute Electron Density and on a Continuum Model of the Solvent Defined by the Bulk Dielectric Constant and Atomic Surface Tensions. *J. Phys. Chem. B* **2009**, *113*, 6378–6396.

(56) Yang, J.; Brookhart, M. Reduction of Alkyl Halides by Triethylsilane Based on a Cationic Iridium Bis(Phosphinite) Pincer Catalyst: Scope, Selectivity and Mechanism. *Adv. Synth. Catal.* **2009**, *351*, 175–187.

(57) Groom, C. R.; Bruno, I. J.; Lightfoot, M. P.; Ward, S. C. The Cambridge Structural Database. *Acta Crystallogr. Sect. B Struct. Sci. Cryst. Eng. Mater.* **2016**, *72*, 171–179.

(58) Wilklow-Marnell, M.; Brennessel, W. W.; Jones, W. D. Reactivity of IPrPCPIrH4 with Para-Benzoquinones. *Polyhedron* **2018**, *143*, 209–214.

(59) Shi, Y.; Suguri, T.; Dohi, C.; Yamada, H.; Kojima, S.; Yamamoto, Y. Highly Active Catalysts for the Transfer Dehydrogenation of Alkanes: Synthesis and Application of Novel 7-6-7 Ring-Based Pincer Iridium Complexes. *Chem. - Eur. J.* **2013**, *19*, 10672–10689.

(60) Siegler, M. A.; Spek, A. L.; Bonnet, S.; Klein Gebbink, R. J. M. CSD Communication (Private Communication), **2015**, CCDC 1443626.

(61) Yao, W.; Jia, X.; Leng, X.; Goldman, A. S.; Brookhart, M.; Huang, Z. Catalytic Alkane Transfer-Dehydrogenation by PSCOP Iridium Pincer Complexes. *Polyhedron* **2016**, *116*, 12–19.

(62) Yang, J.; White, P. S.; Brookhart, M. Scope and Mechanism of the Iridium-Catalyzed Cleavage of Alkyl Ethers with Triethylsilane. *J. Am. Chem. Soc.* **2008**, *130*, 17509–17518.

(63) Huang, Z.; White, P. S.; Brookhart, M. Ligand Exchanges and Selective Catalytic Hydrogenation in Molecular Single Crystals. *Nature* **2010**, *465*, 598–601.

(64) Paul, U. S. D.; Braunschweig, H.; Radius, U. Iridium-Catalysed Dehydrocoupling of Aryl Phosphine–Borane Adducts: Synthesis and Characterisation of High Molecular Weight Poly(Phosphinoboranes). *Chem. Commun.* **2016**, *52*, 8573–8576.

(65) Hebden, T. J.; Denney, M. C.; Pons, V.; Piccoli, P. M. B.; Koetzle, T. F.; Schultz, A. J.; Kaminsky, W.; Goldberg, K. I.; Heinekey, D. M. σ-Borane Complexes of Iridium: Synthesis and Structural Characterization. *J. Am. Chem. Soc.* **2008**, *130*, 10812–10820.

(66) Göttker-Schnetmann, I.; White, P. S.; Brookhart, M. Synthesis and Properties of Iridium Bis(Phosphinite) Pincer Complexes (*p*-XPCP)IrH_2, (*p*-XPCP)Ir(CO), (*p*-PCP)Ir(H)(Aryl), and {(*p*-XPCP)Ir}$_2${μ-N_2} and Their Relevance in Alkane Transfer Dehydrogenation. *Organometallics* **2004**, *23*, 1766–1776.

(67) Rösler, S.; Obenauf, J.; Kempe, R. A Highly Active and Easily Accessible Cobalt Catalyst for Selective Hydrogenation of C═O Bonds. *J. Am. Chem. Soc.* **2015**, *137*, 7998–8001.

(68) Das, S.; Pati, S. K. Mechanistic Insights into Catalytic CO_2 Hydrogenation Using Mn(I)-Complexes with Pendant Oxygen Ligands. *Catal. Sci. Technol.* **2018**, *8*, 3034–3043.

(69) Kar, S.; Kothandaraman, J.; Goeppert, A.; Prakash, G. K. S. Advances in Catalytic Homogeneous Hydrogenation of Carbon Dioxide to Methanol. *J. CO2 Util.* **2018**, *23*, 212–218.

(70) Hou, C.; Li, Y.; Ke, Z. Transition Metal Center Effect on the Mechanism of Homogenous Hydrogenation and Dehydrogenation. *Inorganica Chim. Acta* **2020**, *511*, 119808.

(71) Titova, E. M.; Silantyev, G. A.; Filippov, O. A.; Gulyaeva, E. S.; Gutsul, E. I.; Dolgushin, F. M.; Belkova, N. V. PCP Pincer Iridium Chemistry – Coordination of Pyridines to [(TBuPCP)IrH(Cl)]. *Eur. J. Inorg. Chem.* **2016**, *2016*, 56–63.

(72) Goldberg, J. M.; Cherry, S. D. T.; Guard, L. M.; Kaminsky, W.; Goldberg, K. I.; Heinekey, D. M. Hydrogen Addition to (Pincer)Ir^I(CO) Complexes: The Importance of Steric and Electronic Factors. *Organometallics* **2016**, *35*, 3546–3556.

(73) Goldberg, J. M.; Wong, G. W.; Brastow, K. E.; Kaminsky, W.; Goldberg, K. I.; Heinekey, D. M. The Importance of Steric Factors in Iridium Pincer Complexes. *Organometallics* **2015**, *34*, 753–762.

(74) Kaljurand, I.; Kütt, A.; Sooväli, L.; Rodima, T.; Mäemets, V.; Leito, I.; Koppel, I. A. Extension of the Self-Consistent Spectrophotometric Basicity Scale in Acetonitrile to a Full Span of 28 p K_a Units: Unification of Different Basicity Scales. *J. Org. Chem.* **2005**, *70*, 1019–1028.

(75) Zall, C. M.; Linehan, J. C.; Appel, A. M. A Molecular Copper Catalyst for Hydrogenation of CO_2 to Formate. *ACS Catal.* **2015**, *5*, 5301–5305.

(76) Pratt, R. C.; Lohmeijer, B. G. G.; Long, D. A.; Waymouth, R. M.; Hedrick, J. L. Triazabicyclodecene: A Simple Bifunctional Organocatalyst for Acyl Transfer and Ring-Opening Polymerization of Cyclic Esters. *J. Am. Chem. Soc.* **2006**, *128*, 4556–4557.

(77) Kiesewetter, M. K.; Scholten, M. D.; Kirn, N.; Weber, R. L.; Hedrick, J. L.; Waymouth, R. M. Cyclic Guanidine Organic Catalysts: What Is Magic About Triazabicyclodecene? *J. Org. Chem.* **2009**, *74*, 9490–9496.

(78) Mutlu, H.; Ruiz, J.; Solleder, S. C.; Meier, M. A. R. TBD Catalysis with Dimethyl Carbonate: A Fruitful and Sustainable Alliance. *Green Chem.* **2012**, *14*, 1728.

(79) Von Wolff, N.; Lefèvre, G.; Berthet, J.-C.; Thuéry, P.; Cantat, T. Implications of CO_2 Activation by Frustrated Lewis Pairs in the Catalytic Hydroboration of CO_2: A View Using N/Si^+ Frustrated Lewis Pairs. *ACS Catal.* **2016**, *6*, 4526–4535.

(80) Zhao, J. Oxidative Addition of Ammonia to Form a Stable Monomeric Amido Hydride Complex. *Science* **2005**, *307*, 1080–1082.

(81) Titova, E. M.; Silantyev, G. A.; Filippov, O. A.; Gulyaeva, E. S.; Gutsul, E. I.; Dolgushin, F. M.; Belkova, N. V. PCP Pincer Iridium Chemistry - Coordination of Pyridines to [(^{tBu}PCP)IrH(Cl)]: Coordination of Pyridines to [(^{tBu}PCP)IrH(Cl)]. *Eur. J. Inorg. Chem.* **2016**, *2016*, 56–63.

(82) Adams, J. J.; Arulsamy, N.; Roddick, D. M. Acceptor PCP Pincer Iridium(I) Chemistry: Stabilization of Nonmeridional PCP Coordination Geometries. *Organometallics* **2011**, *30*, 697–711.

(83) Zuckerman, J. J., In *Inorganic Reactions and Methods. 14: Formation of Bonds to Transition and Inner Transition Metals; Wiley*, ***1998***, *pp 249–318.*